SYNOPTIC ANALYSIS AND NUMERICAL MODELLING OF AN EXPLOSIVELY DEEPENING CYCLONE

RICHARD J. REED[1]
Department of Atmospheric Sciences
University of Washington
Seattle, Washington U.S.A

Summary: This paper describes an extraordinary explosive cyclogenesis that occurred in the eastern Pacific in November 1981 and the results of simulations of the storm development carried out with the Penn State/NCAR Mesoscale Model Version 4 (MM4). The model simulations give a realistic portrayal of the storm development and suggest that moist symmetric instability was the key factor in the rapid deepening.

1. INTRODUCTION

In November 1981 an extreme case of explosive cyclogenesis occurred in a section of the Eastern Pacific that is known from climatological data (Roebber, 1984) to be a region where such events are relatively rare. Between 0000 GMT 13 November and 0000 GMT 14 November the storm deepened nearly 50 mb. Deepening rates of approximately 40 mb $(12h)^{-1}$ and 30 mb $(6h)^{-1}$ were observed within the 24h period. Several ships caught in the storm registered winds of 25 m s^{-1} or greater and two ships reported speeds in excess of 45 m s^{-1}.

As will be shown subsequently, at least one of the operational forecast models - the U.S. National Meteorological Center's Limited-area, fine-mesh model (LFM) - completely failed to predict the development. This failure, coupled with the relative simplicity of the large-scale flow pattern within which the development took place, has made this a particularly attractive case for study.

This paper has two main objectives: first to present a brief synoptic description of the event (a full description can be found in Reed and Albright, 1986) and second to describe the results of numerical experiments

[1] The numerical modelling work described herein was led by Dr. Ying-Hwa Kuo, National Center for Atmospheric Research (NCAR), Boulder, Colorado, U.S.A.

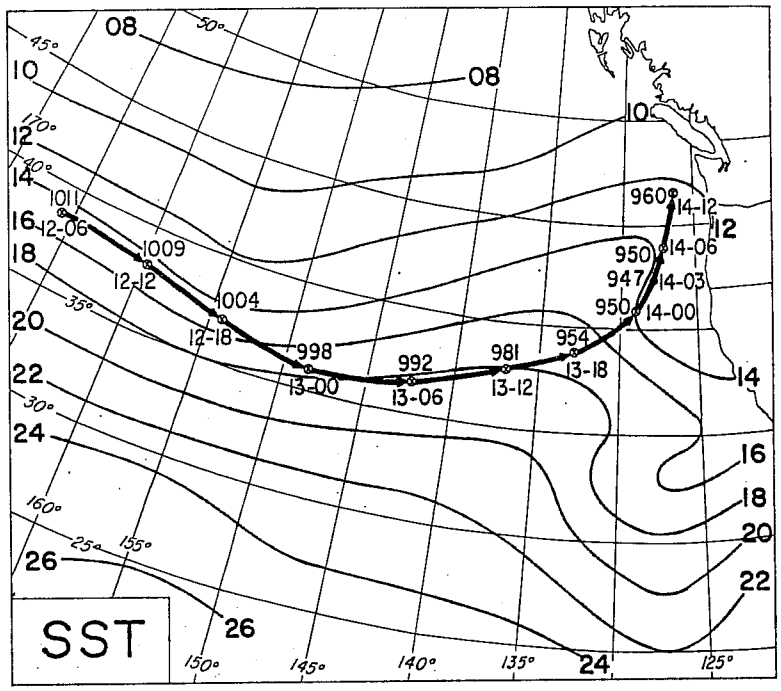

Fig. 1. Sea surface temperatures (°C) 0000 GMT 12 November to 1200 GMT 14 November 1981, and storm track with 6h positions and corresponding central pressures of the low.

carried out with the Penn State/NCAR Mesoscale Model Version 4 (MM4). The aims of the experiments were (1) to test the ability of the MM4 model to simulate the event and (2) to elucidate the roles of various physical mechanisms in the storm development.

2. SYNOPTIC DESCRIPTION

The storm path and intensity (central pressure) during the period from 0600 GMT 12 November to 1200 GMT 14 November 1981 appear in Fig. 1. The disturbance was an offshoot of an earlier, moderately intense, occluded cyclone that stagnated and filled in the Western Pacific. It began as a wave on the warm front of the occlusion, was steered around a large-scale quasi-stationary ridge centered near the dateline and at the time of the initial position shown in Fig. 2a was moving rapidly east-southeastward to the rear of a long-wave trough. The storm deepened moderately at first while maintaining a speed of 25 m s^{-1}. Rapid deepening ($\geq$ 6 mb $(6\ h)^{-1}$) commenced at 1800 GMT 12 November; extreme explosive deepening of 27 mb $(6h)^{-1}$ occurred between 1200 and 1800 GMT 13 November as the storm movement slowed to about 15 m s^{-1}. Because of a deficiency of ship reports at 1200 GMT 13 November, it is possible that the central pressure at that hour was

lower than 981 mb and the deepening rate accordingly less. However, considerable confidence is felt in the 38 mb deepening estimated for the 12h period centered on that time. The maximum depth of 947 mb was attained at 0300 GMT 14 November while the storm was still moving at 15 m s^{-1}.

The analysis of sea-surface temperature (SST) also shown on Fig. 1, reveals that the development took place in a region of moderate to warm SST's and at most moderate (at least by western ocean standards) SST gradients.

A sequence of surface, 500 mb and 250 mb charts depicting the storm development during the 24h period of most rapid deepening appears in Figs. 2a-i. The surface chart for 0000 GMT 13 November (Fig. 2a) shows a small wave cyclone with a sharp cold front and diffuse warm front. Numerous ship reports confirm the isobaric analysis. Unusually strong baroclinity, as evidenced by the 1000-500 mb thickness analysis, is present in a broad zone about the low. A broad large-scale trough exists at 500 mb (Fig. 2b) within which two secondary vorticity maxima are seen, one upstream of the surface low (circled cross). Weak to moderate positive vorticity advection (PVA) is present over the low center. The 250 mb chart (Fig. 2c) is marked by a strong jet stream with a maximum speed of 97 m s^{-1} occurring upstream of the trough. This extreme velocity gives further evidence of the strong baroclinity.

By 1200 GMT 13 November (Fig. 2d) the low has undergone considerable deepening. Ship reports are lacking near the center of the low. Satellite images (to be shown shortly) are the main basis for the analysis of the inner isobars. Strong baroclinity continues over a wide region about the low. The 500 mb chart (Fig. 2e) shows a strong amplification of the upper-level trough and a considerably enhanced vorticity maximum. The low, which earlier was located beneath the jet axis, has now crossed to the cyclonic side (Fig. 2f). The jet maximum - quite well defined by aircraft winds (not plotted) - has declined considerably.

The surface map for 0000 GMT 14 November (Fig. 2g), drawn to the same scale as the previous surface maps, shows the intense development that took place during the 12h period. The analysis is based on numerous ship and buoy reports which have been omitted for clarity. (They can be found in Fig. 11b of Reed and Albright, 1986.) The 500 mb chart (Fig. 2h) indicates

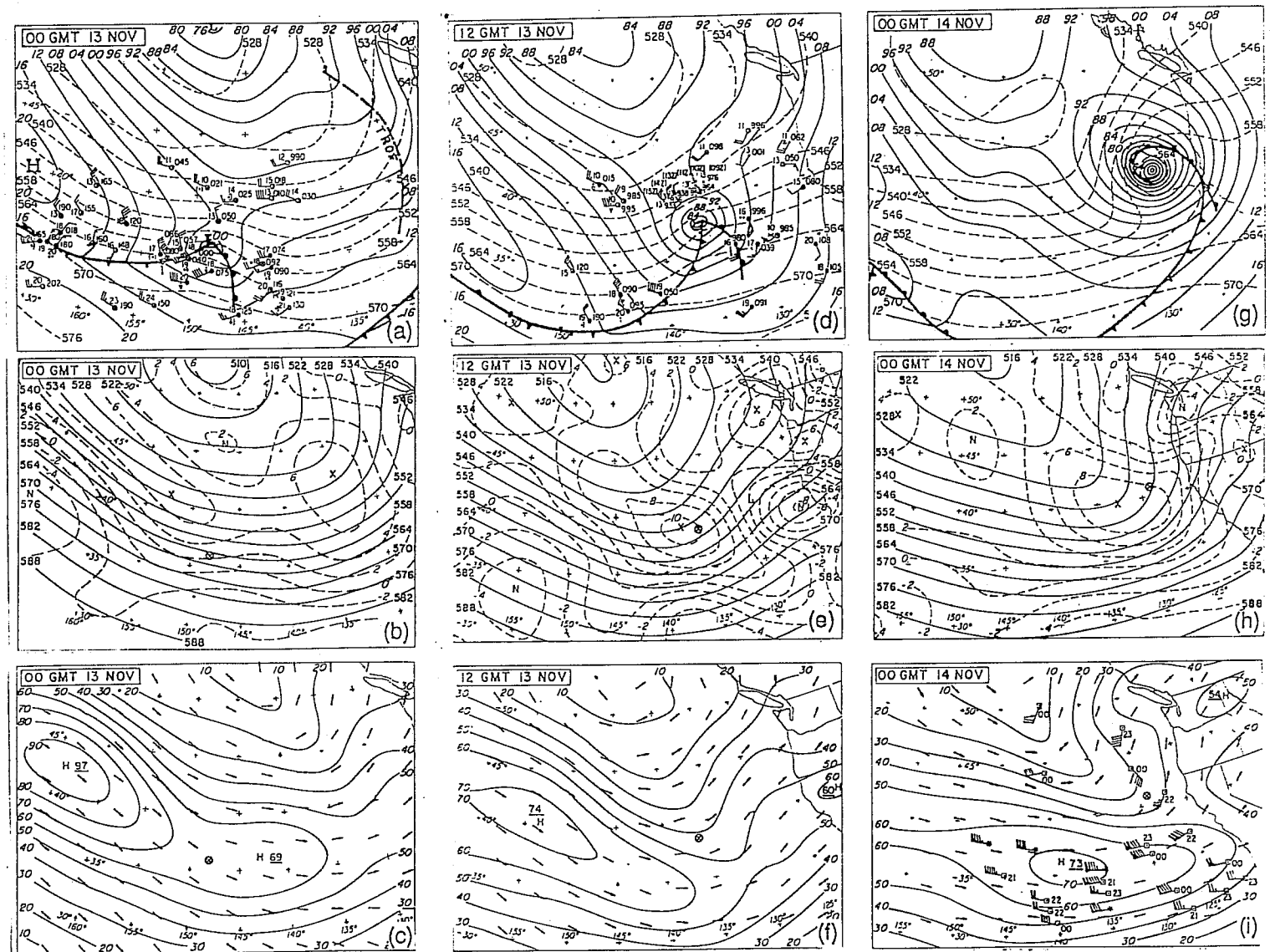

Fig. 2. Surface map (isobars and 1000-500 mb thickness in dam) 500 mb map (contours in dam and relative vorticity in 10^{-5} s^{-1}) and 250 mb map (wind direction and magnitude in m s^{-1}) at 0000 GMT 13 November (a,b,c), 1200 GMT 13 November (d,e,f) and 0000 GMT 14 November (g,h,i). Symbols have usual meaning.

little further strengthening of the 500 mb trough, unlike the ECMWF analysis (not shown) which, almost certainly more correctly, shows a further increase in the vorticity aloft. The combination of an intense, circular low at the surface and open trough aloft produces a warm core in the 1000-500 mb thickness (Fig. 2g). The reality of this feature will be discussed later. The surface temperature analysis they show reveals intertwining warm and cold tongues near the center, not a pool of warm air.

The NMC/NCAR analysis of a broad open trough at 500 mb is made especially questionable by aircraft winds plotted on the correspondingly 250 mb chart (Fig. 2i). Note particularly the 20 m s^{-1} southeast wind to the northwest of the surface low position (circled cross) at a location where the NMC/NCAR analysis indicates a southwest wind of 30 m s^{-1}. We will see later that the MM4 24h forecast is in better agreement with the aircraft winds than the analysis! In any event it is evident that the analysis underestimates the strength of the upper-level trough (or closed low).

Satellite pictures of the development appear in Figs. 3a-e. A GOES-W visible image for 2115 GMT (Fig. 3a) reveals a leaf-shaped frontal cloud band embedded within a convective cloud field. The low static stability of the large-scale environment is evident from the widespread convection. The appearance of a comma-shaped pattern with dry slot and convective tail in the IR image for 0615 GMT (Fig. 3b) signals the start of the explosive deepening. By 1215 GMT (Fig. 3c) the comma head is well developed and a striking "black hole" of very low mid and upper tropospheric relative humidity is seen to the southwest of the low center in the water vapor imagery. An IR image for 1645 GMT 13 November (Fig. 3d) and a visible image for 2215 GMT (Fig. 3e) show the transition from the comma-shaped cloud pattern to a spiral-shaped pattern with intertwining warm moist and cool dry air in the vicinity of the storm center.

Meridional cross sections constructed along 147°W at 0000 GMT 13 November, just ahead of the low center (Fig. 2a), appear in Figs. 4a and b. The potential isotherms and isotachs of the zonal wind in Fig. 4a illustrate the broad and deep baroclinity that existed prior to and during the rapid deepening phase. A relatively shallow region with sharp front-like features is also evident. Equally revealing from the dynamical standpoint is the cloud and thermodynamic structure depicted in Fig. 4b. The

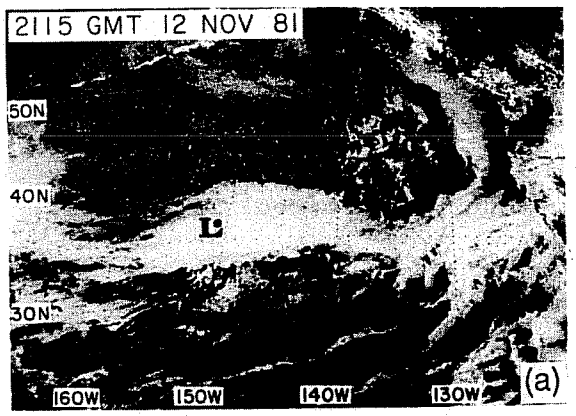

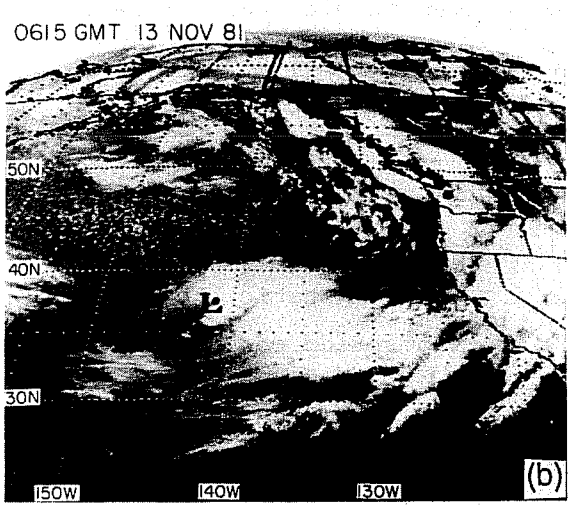

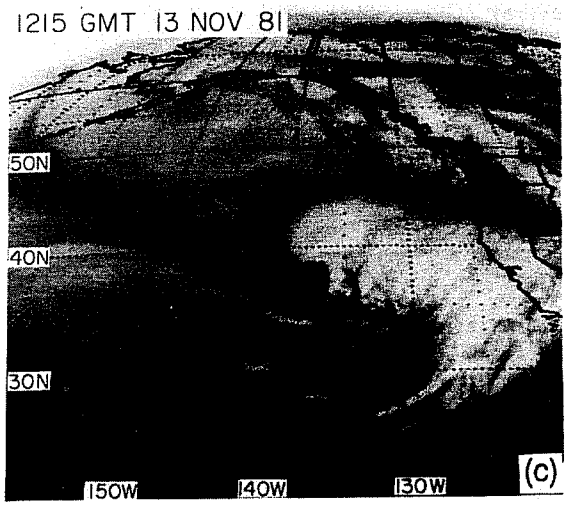

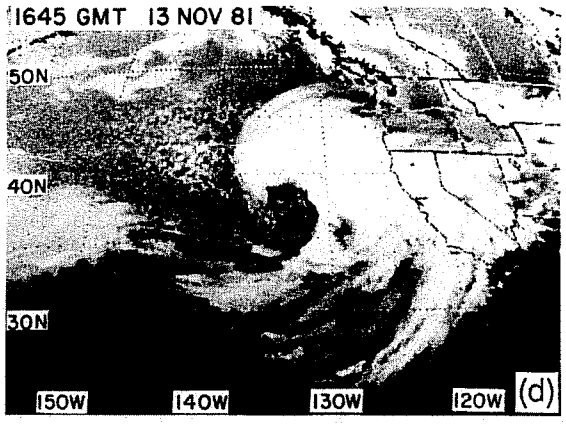

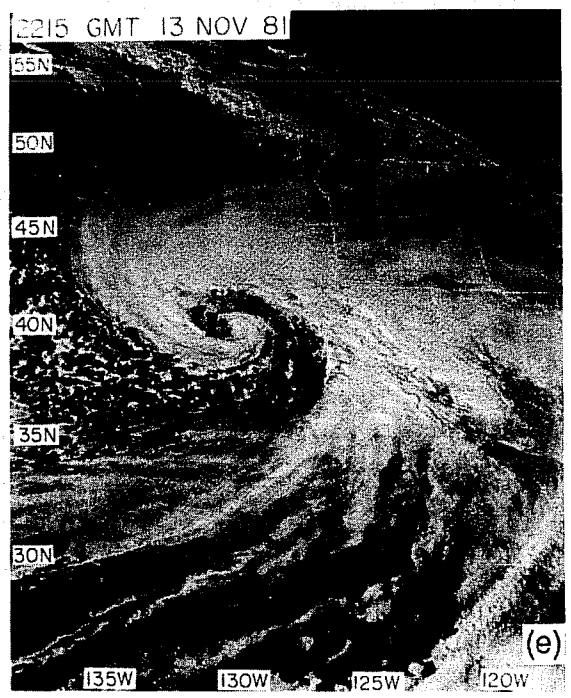

Fig. 3. GOES-W satellite images: (a) visible, 2115 GMT 12 November, (b) IR, 0615 GMT 13 November, (c) water vapor channel, 1215 GMT 13 November, (d) IR, 1645 GMT 13 November and (e) visible, 2215 GMT 13 November.

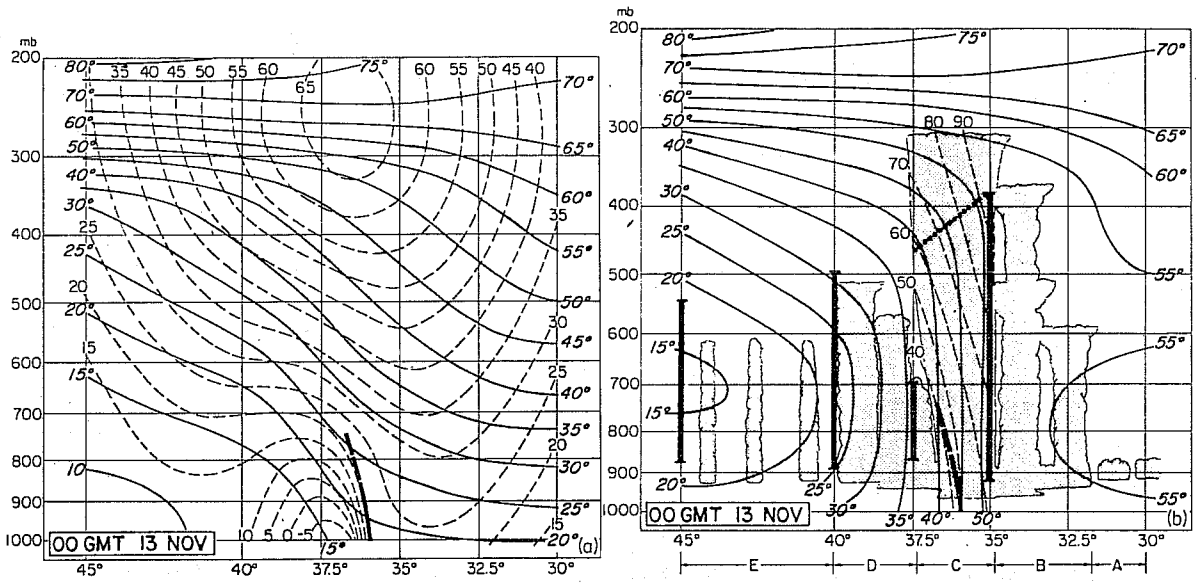

Fig. 4. Cross sections along 147.5°W at 0000 GMT 13 November: (a) Potential isotherms (°C), solid; isotachs (m s^{-1}) of normal wind component, dashed. Heavy line denotes front. (b) Equivalent potential temperture (°C) solid; absolute momentum (m s^{-1}), dashed. Shading denotes clouds. Heavy bars give depth of region of positive buoyancy for lifted surface parcels. Large dots indicate top of zone of symmetric instability.

isopleths of equivalent potential temperature, Θ_E, (solid lines) are essentially vertical in the frontal cloud band, indicative of neutral static stability. Potential instability to heights of 800-700 mb exists on either side of the band. Cloud tops to 700-500 mb are indicated by the depth of the positive area (heavy bars) on a thermodynamic diagram.

Perhaps most revealing is the indicated presence of symmetric instability in the frontal band. This can be inferred from the orientation of the dashed lines of absolute momentum M, defined as M = u - fy (Eliassen, 1962). Along these lines θ_E decreases upward, a condition conducive to slantwise convection (Bennetts and Hoskins, 1979; Emanuel, 1983). Within this zone vigorous frontal upglide along sloping surfaces (Thorpe and Emanuel, 1985) and associated spin-up of surface vorticity is suggested.

We close the synoptic description by showing the initial LFM analysis at 0000 GMT 13 November (Fig. 5a) and the 24h forecast for 0000 GMT 14 November (Fig. 5b). Because of the lack of ship reports at the time the forecast was run, the surface low was badly analyzed (see Fig. 2a). The prognostic chart gives no evidence of the low. The 24h forecast was in error by 55 mb at the observed position of the center (circled cross in Fig. 5b).

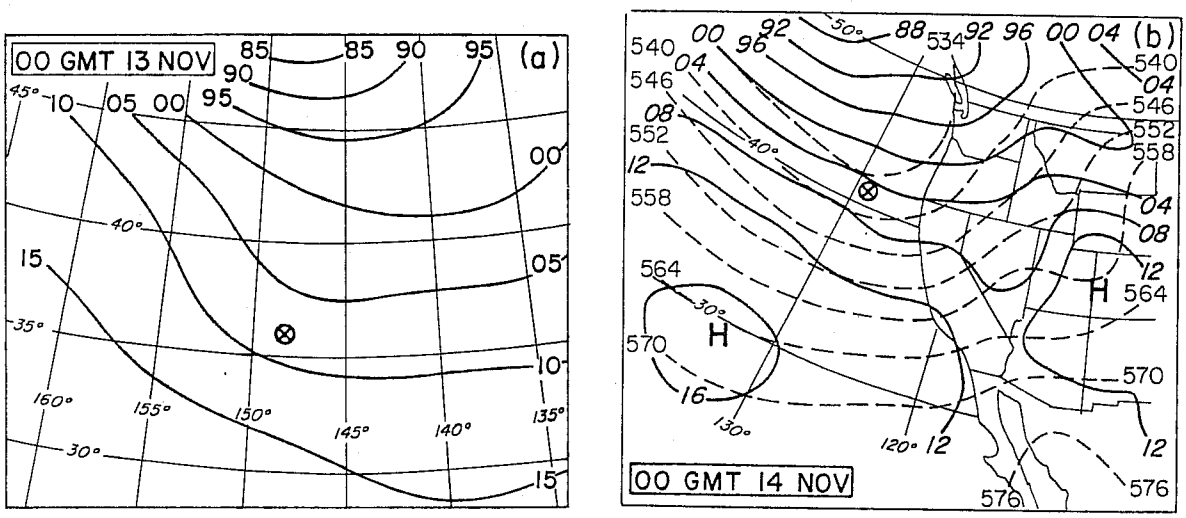

Fig. 5. (a) NMC final surface analysis for 0000 GMT 13 November (b) LFM forecast verifying at 0000 GMT 14 November. Cross indicates position of low center.

3. MODEL EXPERIMENTS

3.1 Model description and experimental design

A full description of the MM4 model is contained in an NCAR Technical Note (Anthes et al., 1987). In the present experiments the model was run on a 91 x 121 grid with horizontal resolution of 40 km and 15 layers in the vertical defined in a σ coordinate system. A sub-area of the forecast domain is used in the subsequent presentation of forecast results. Boundary conditions for the model were interpolated spatially and temporally from 12 hourly NMC analyses. A leapfrog scheme with a 75s time step was used in the integrations. Smoothing was accomplished and computational stability maintained by a fourth order diffusion scheme. Model physics incorporated in the experiments included (1) Surface and planetary boundary layer (PBL) fluxes of heat and moisture based on the High-Resolution Blackadar Model (Blackadar, 1979; Zhang and Anthes, 1982), (2) above the mixed layer, vertical diffusion according to a K-theory formulation, (3) cloud-radiation interaction and (4) a water cycle with option for either explicit (grid-point) or parameterized (sub grid point) precipitation. The explicit scheme involves prognostic equations for water vapor, cloud water and rain water (Hsie, et al., 1984); the convective parameterization scheme employs the Anthes modification of the Kuo scheme (Anthes et al., 1987) and a diagnostic relationship for the non-convective precipitation. Sea surface temperatures required for surface flux

calculations were taken from regularly updated fields disseminated by the U.S. National Meteorlogical Center.

The experimental design is summarized in Table 1. Six experiments, including the control experiment, were carried out. All forecasts or simulations were initialized at 0000 GMT 13 November and were run for 48 hrs. Results for the first 24 hours only are shown. The control experiment (Exp. 1) included surface fluxes, friction and the explicit prediction of water vapor, cloud water and rain water on the grid scale

Table 1. Summary of Numerical Experiments

Exp. No.	surface fluxes	surface friction	hydrological cycle
1	yes	yes	explicit scheme
2	no	yes	explicit scheme
3	yes	yes	cu. par. + non-conv. par.
4	yes	yes	passive moisture (dry)
5	no	yes	passive moisture (dry)
6	no	no	passive moisture (dry)

without cumulus parameterization. Experiment 2 was identical to the control, except that the surface heat and moisture fluxes were turned off. Experiment 3 was the same as the control, except the moisture cycle was different. It used a cumulus parameterization described in Anthes et al. (1987) along with a parameterization of non-convective precipitation without explicit prediction of cloud water and rain water. In the subsequent simulations, the latent heat release associated with condensation was set to zero, and the water vapor was treated as a passive scalar. In essence these experiments test how much of the development can be ascribed to dry baroclinity. Experiment 4, called the full physics dry run, was the same as the control, except that latent heat release was not included. Experiment 5 was the same as Exp. 4, except that the surface fluxes were removed. In experiment 6, surface friction was removed in addition to the surface energy fluxes.

3.2 Experimental results

First we present results of the control experiment with the purpose of showing how well this experiment reproduced observed features of the development. Next, we consider the results of the sensitivity experiments

that look into the roles of various physical mechanisms. Finally, we present diagnostic results that show the mechanism responsible for the rapid intensification in the control experiment.

3.2.1. Results of the control experiment

Fig. 6 compares predicted and observed tracks and intensities of the storm during the 24h period. It is evident that the predicted track was somewhat to the right of (south and east of) the observed track, but the discrepancy is small. The storm travelled more than 1800 km in the 24h period; the predicted position at the end of the period was in error by only 150 km. Although the predicted storm did not attain the observed depth of 950 mb, the central pressure did reach an unusually low value (969 mb). In brief, the storm movement was well predicted in the control experiment and rapid deepening (31 mb $(24h)^{-1}$) was successfully predicted, though the deepening was considerably less than that observed (48 mb $(24h)^{-1}$).

Prognostic surface and 500 mb charts for 1200 GMT 13 November and 0000 GMT 14 November are shown in Figs. 7a-d. We have chosen to depict isotherms on the 500 mb prognostic charts rather than the vorticity isopleths shown on

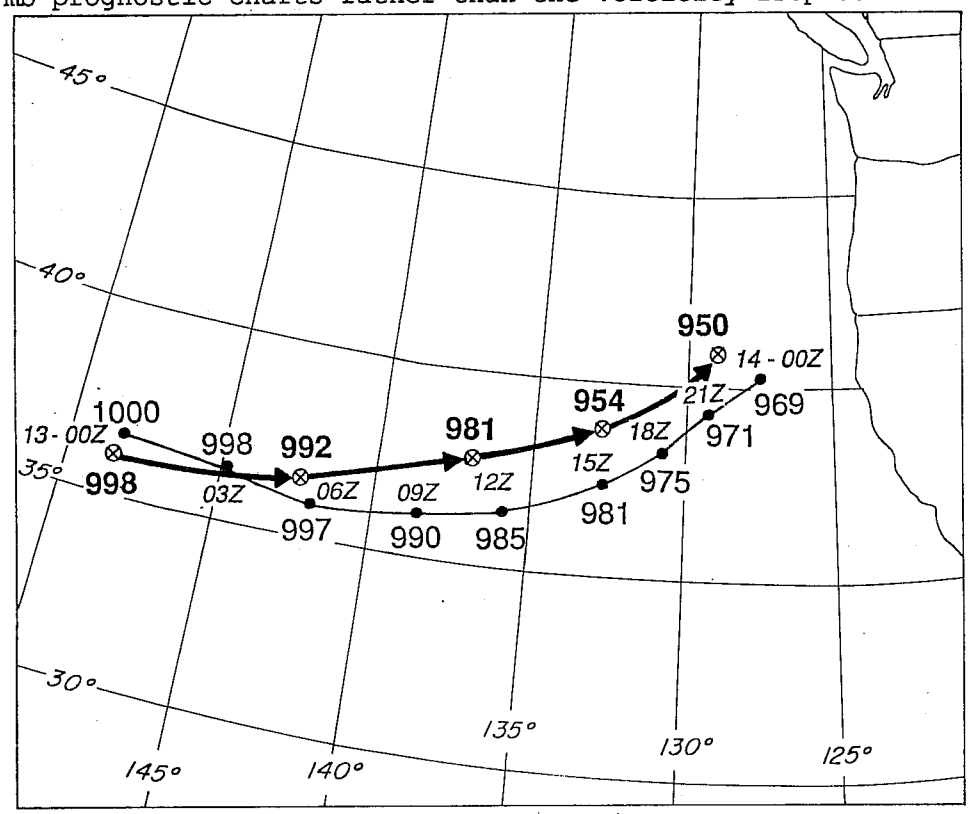

Fig. 6. Comparison of predicted path (dots) and central pressure of the low with the observed path (circles) and central pressure. Positions every 3h for the predicted storm and 6h for the observed.

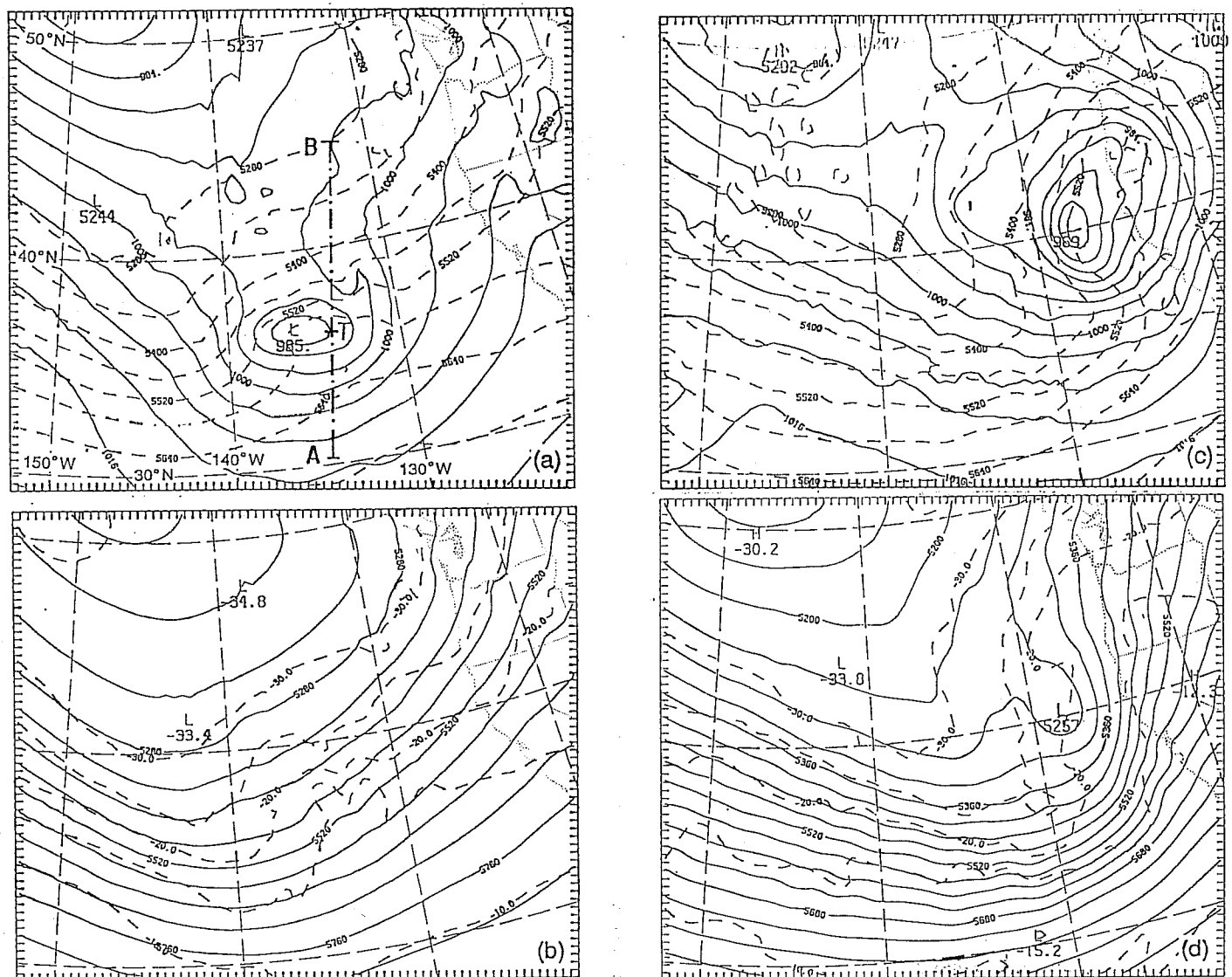

Fig. 7. 12h forecast for control experiment verifying at 1200 GMT 13 February of (a) surface pressure, solid, and 100-500 mb thickness, dashed, and (b) 500 mb height (m), solid, and temperature (°C), dashed, and (c) and (d) 24h forecasts verifying at 0000 GMT 14 February.

the 500 mb analyses (Figs. 2d-f). The predicted surface pressure pattern for 1200 GMT with superimposed 1000-500 mb thickness (Fig. 7a) compares favorably with the observed (Fig. 2d). As seen on this and later charts, the use of the explicit scheme results in a rather noisy pattern, which is caused by shallow convection in association with strong surface energy fluxes. The small-scale features are not of concern here and will be ignored in further discussions. The 500 mb chart for 1200 GMT (Fig. 7b) broadly resembles the analysis (Fig. 2e). A tendency for the trough to split in the region immediately to the south and west of the surface low center can be noted. Another noteworthy feature is the tongue of warm air and pronounced temperature gradient situated to the northeast of the low center. It is speculated that this feature is produced, at least in part, by latent heat release. The feature is much less pronounced in the dry runs (not shown).

The 24h surface forecast (Fig. 7c) shows the low to be well positioned but, as stated previously, not sufficiently deep. Unlike the observed low, which is circular in shape (Fig. 2g), the predicted low is elongated to the northeast. The thickness pattern reveals that the elongation was associated with warm frontogenesis in the northeast sector. Thus the forecast failed to capture the development of the tight inner core of the cyclone with its intertwined tongues of warm and cold air. This failure may have been caused in part by insufficient grid resolution. The 500 mb forecast for 0000 GMT on the 14th (Fig. 7d) shows the dual nature of the trough, noted previously. Indeed a mesoscale low center exists almost directly over the surface low. This feature is lacking in the analysis (Fig. 2b). However, it may well be a real feature, since no middle level data were available in the region in question and the aircraft winds at higher levels showed that the 250 mb analysis (Fig. 2i) considerably underestimated the amplitude of the upper-level trough. Note that because of the upper mesoscale low, the 1000-500 mb thickness chart (Fig. 7c) does not possess the perhaps unrealistic warm core seen in Fig. 2g.

It was suggested earlier, and immediately above, that the predicted upper-level winds for 0000 GMT 14 November were in better agreement with the aircraft winds than were the analyzed winds (Fig. 2i). In support of this contention we present in Fig. 8a the forecasted flow field at 300 mb with three of the pertinent aircraft winds plotted. The 20 m s^{-1} southeasterly

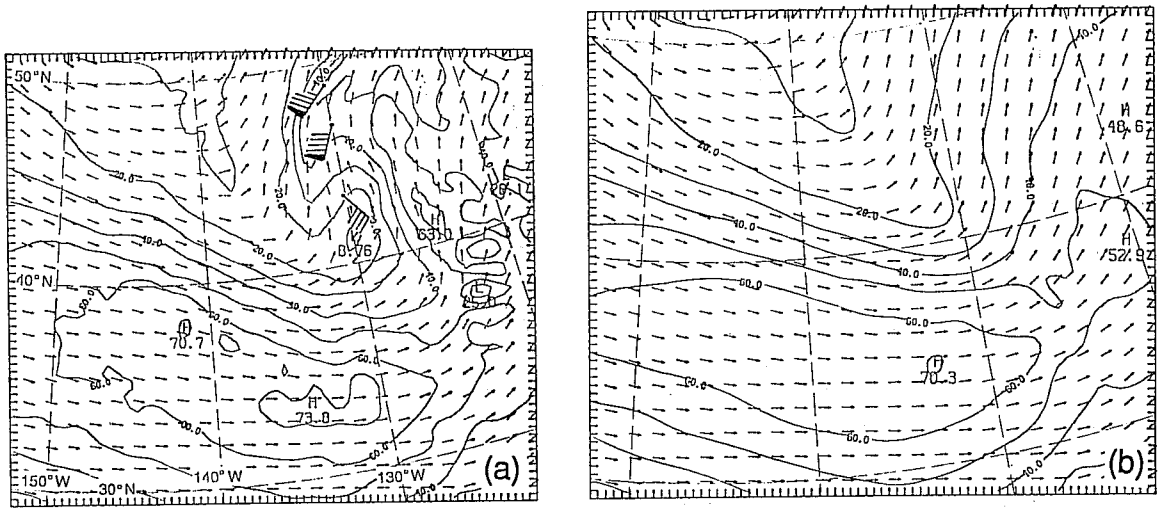

Fig. 8. (a) 24h forecast for control experiment of 300 mb wind field verifying at 0000 GMT 14 November. Isotachs in m s^{-1}. (b) Same for "dry" experiment. Wind plots in (a) show aircraft measurements taken within 1h of 0000 GMT. Pennant, 25 m s^{-1}; full barb 5 m s^{-1}.

aircraft wind immediately to the north-northwest of the low center clearly fits the forecast better than the analysis (Fig. 2i). Likewise the approximately 45 m s^{-1} southwesterly winds further to the north fit the prediction better.

The importance of latent heat release in producing the sharp trough and wind minimum at 300 mb in the vicinity of the low and the pronounced downstream ridge with strong winds can be seen by comparing Fig. 8a with Fig. 8b, the corresponding 300 mb wind field from experiment 4, the full physics dry run. Without the latent heat addition the trough and ridge are less accentuated and the strong wind increase aloft downstream of the low disappears.

The predicted fields of relative humidity at 400 mb for 1500 GMT 13 November and 0000 GMT 14 November are shown in Figs. 9a and b. Areas with relative humidity less than 80 percent are shaded. These areas are presumably free of cold clouds and should appear dark on unenhanced infrared satellite images (and also on visible images if the coverage by low clouds is not large). Thus the remaining white areas should conform to the middle and upper level cloud patterns appearing in the images. Distinctive features of Fig. 9a are (1) the sharp outer cloud edge of the storm, (2) the exceedingly low humidities near and south of the storm center that connect westward to an elongated region of low humidity and (3)

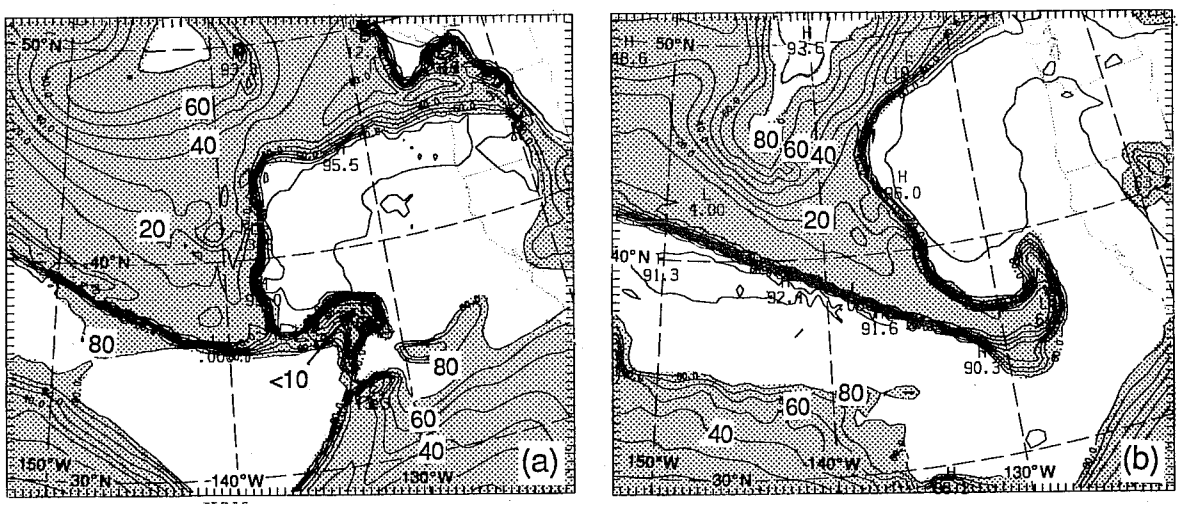

Fig. 9. (a) 15h forecast verifying at 1500 GMT 13 February of 400 mb relative humidity. (b) 24h forecast verifying at 0000 GMT 14 February. Areas with R.H. less than 80 per cent are shaded.

the large elongated region of high humidities intruding from the west. The sharp outer boundary to the cloud mass of the main storm is again evident at 0000 GMT 14 November (Fig. 9b), displaced north and east of its earlier position. The dry corridor from the west is even more evident at the later hour and has taken on a hook shape in the vicinity of the low center. The moist region or cloud mass approaching from the west has merged with the cloud system of the storm.

Although these features are not perfectly reproduced in the satellite imagery (Fig. 3), the general agreement between the moisture field and observed cloud pattern is remarkable. If allowance is made for the 3h time difference, the "black hole" in the water vapor imagery (Fig. 3c) corresponds well with the extreme humidity minimum in Fig. 9a. Again, with minor time adjustments, the outer cloud boundary in Figs. 3d and e agrees with the boundary inferred from the humidity predictions. The dry corridor is somewhat narrower than suggested by the satellite imagery, but its axis is well placed. Figs. 3c-e indicate the approach of a new storm from the upstream direction. Figs. 3c and e in particular confirm the merging of the high level moisture and cloud patterns of the second low with those of the first.

3.2.2 Results of the sensitivity experiments

Results of the sensitivity experiments are shown in Fig. 10a, which depicts the central pressure of the storm during the period 0000 GMT 13 November to 0000 GMT 14 November for each of the six experiments and for the observed situation, as given by Reed and Albright (1986). Clearly none of the experiments succeeded in simulating the extraordinary deepening rate observed at, and immediately after, 1200 GMT on the 13th or the full depth of the storm. However, rapid deepening (> 24 mb $(24h)^{-1}$) and the development of a major cyclone (central pressure < 970 mb) were predicted for the three experiments incorporating latent heat release. Of the three experiments, the control experiment exhibited the most rapid deepening and the lowest pressure but only by a small margin. The most rapid deepening occurred earlier in the control experiment than in the experiment with cumulus parameterization. Removal of the surface fluxes from the control experiment had little effect on the storm intensity.

None of the dry experiments reached the 24 mb $(24h)^{-1}$ criterion for rapid deepening, though the frictionless case came close. In keeping with baroclinic theory, surface fluxes were of little consequence during the rapidly deepening stage, though unquestionably they must have been of importance in creating the favorable large scale environment that allowed the event to occur.

Similar conclusions are reached from the time traces of the 925 mb vorticity maximum for the various experiments (Fig. 10b). Relative vorticities in excess of 6 times the earth's vorticity were achieved in the experiments with latent heat release. The earlier intensification of the storm in the control experiment than in the experiment with cumulus parameterization is even more apparent in the vorticity than it was in the pressure.

3.2.3 The mechanism of rapid deepening in the control run

The meridional cross section taken just in advance of the storm center at 0000 GMT 13 November (Fig. 4b) revealed that near neutral static stability was present in the frontal cloud band from cloud base to about 500-400 mb and that symmetric instability was also present in the cloud band at the same levels. It is of interest to examine the stability conditions at a similar position with respect to the low center at 1200 GMT 13 November, as

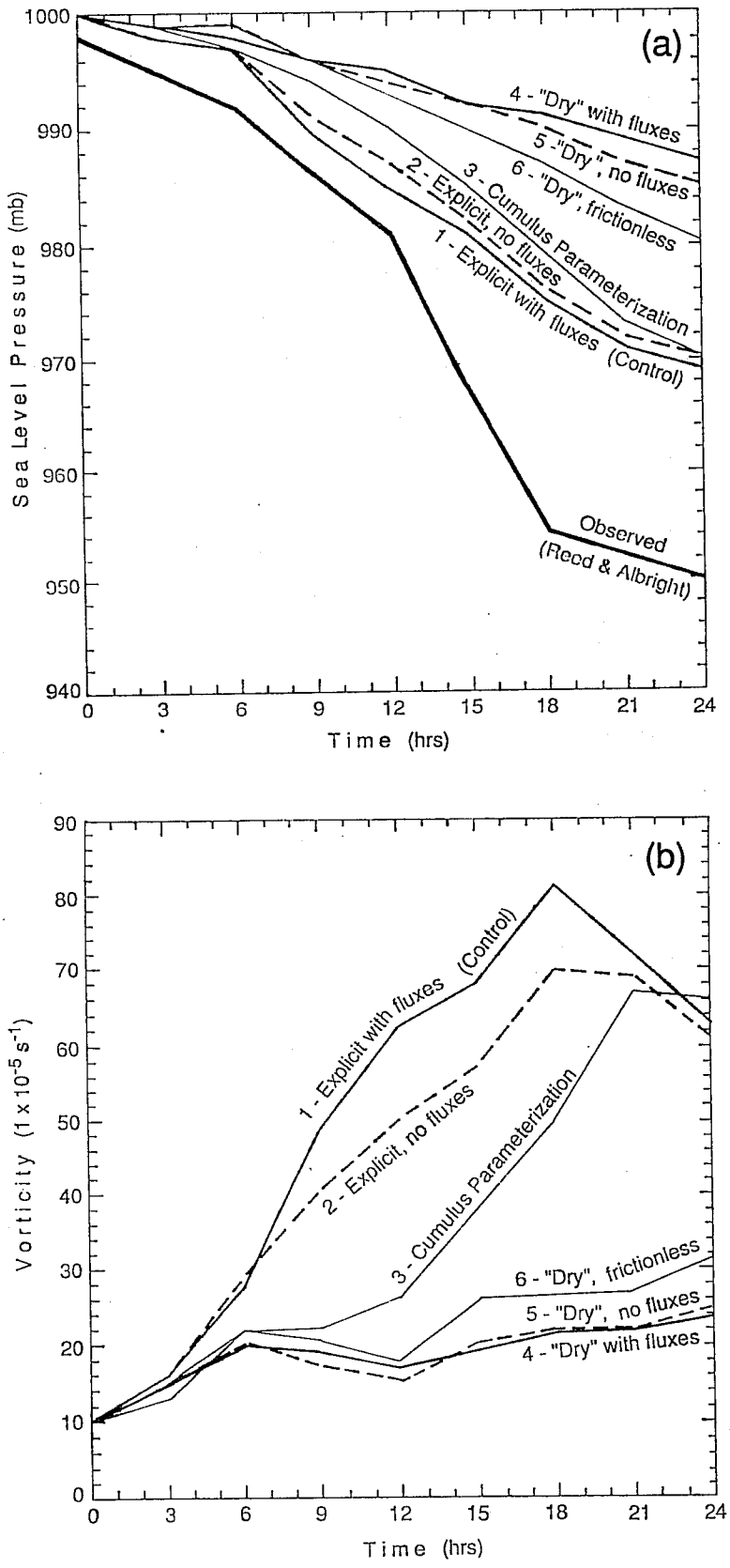

Fig. 10. (a) Central pressure of low, beginning at 0000 GMT 13 November, for the six experiments. (b) Same for the 925 mb vorticity maximum.

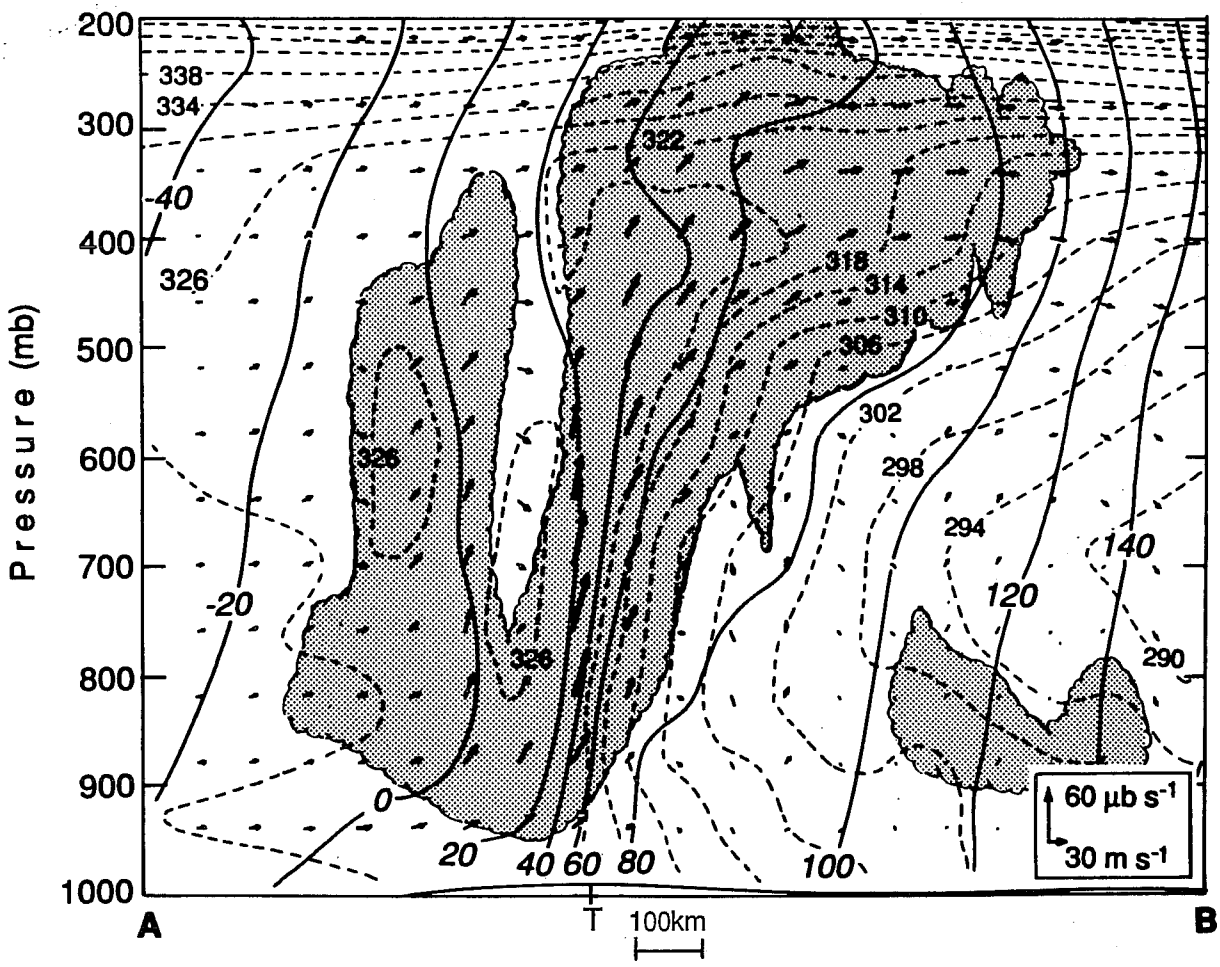

Fig. 11. Cross section along the line AB in Fig. 7a of absolute momentum (solid) and equivalent potential temperture, dashed, at 1200 GMT 13 November. Arrows give flow in plane of cross section according to the attached scale. Shading denotes cloud mass.

revealed by the 12h forecast. The structure at that hour, when the storm was in its most rapidly deepening phase, appears in Fig. 11. The figure shows the two-dimensional motion in the plane of the cross section in addition to the θ_E- and M-lines. The stippling denotes region of cloud as deduced from the field of cloud water (not shown). The position of the cross section is marked by the dash-dot line in Fig. 7a.

The cross section shows that the air is weakly statically stable throughout most of the cloud band and that it is symmetrically neutral (θ_E-lines parallelling M-lines) or slightly symmetrically unstable (θ_E-lines more steeply sloped than M-lines). Within the zone of neutral symmetric stability, the velocity vectors indicate the existence of a narrow sloping sheet of rapidly ascending air. Maximum upward motions are approximately 75 cm s^{-1} (70 μb s^{-1}) within the region of upglide. Upward motion of this

magnitude close to the surface produces strong vertical stretching of boundary layer air and associated strong spin-up of low-level vorticity. It is apparent that, in the model at least, it is the strong, sheet-like ascent made possible by the neutral symmetric stability or slight symmetric instability that is responsible for the rapid intensification of the vortex.

Table 2. Divergences and Vorticities (10^{-4} s^{-1}) along selected trajectories

	A		B		C	
Hour (GMT)	Div.	Vort.	Div.	Vort.	Div.	Vort.
06	.08	-.19	.13	-.10	.50	.00
07	.06	-.20	.11	-.09	.10	-.03
08	-.01	-.20	-.01	-.09	.60	-.04
09	-.08	-.12	-.07	-.03	.70	-.08
10	-.09	-.05	-.37	.07	-.70	-.08
11	-.32	.00	-1.00	.29	-.35	.07
12	-.66	.25	-.70	.59	-.13	.07
13	-1.70	1.70	-1.70	2.70	-1.00	.30
14	-2.50	5.20	-3.40	4.90	-3.10	2.10
15	-.59	7.60	-3.80	7.40	-2.70	6.30

The rapidity with which the vorticity spins up is illustrated in Table 2 which gives hourly values of relative vorticity and convergence for air trajectories that at 1500 GMT 13 February were located at the 925 mb level and at the geographical positions A_o, B_o and C_o in Fig. 12. Pressures at the beginning and end points of the trajectories are appropriately labelled. The chosen points had all acquired relative vorticities in excess of six times the coriolis parameter at the 1500 GMT hour. From the table, it is apparent that the large vorticities were acquired in a brief span - much of the increase occurring in 3-4h. During part of the time the vorticity grew super-exponentially, i.e. the convergence producing the exponential growth was itself growing.

4. CONCLUDING SUMMARY AND REMARKS

In this paper we have presented a case of extraordinary cyclogenesis that occurred in the eastern Pacific in November 1981 and have shown the results of numerical experiments armed at simulating the storm development and

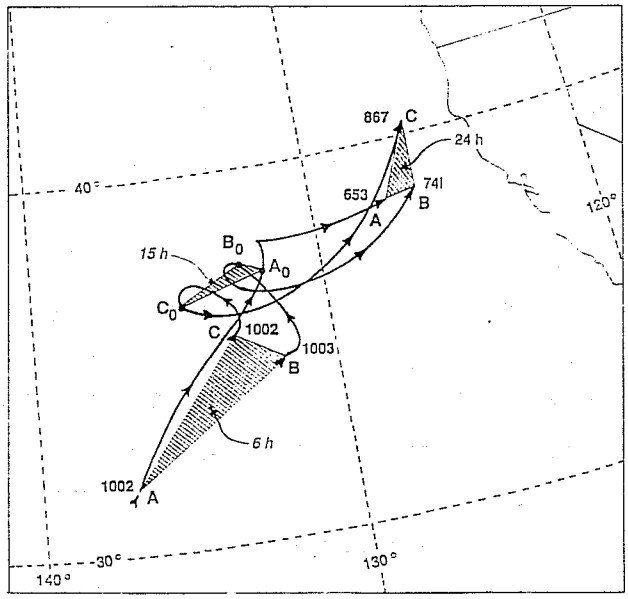

Fig. 12. Trajectories beginning at 0600 GMT 13 November and ending at 0000 GMT 14 November for air parcels that at 1500 GMT 13 November were located at points A_o, B_o, C_o and 925 mb. Enclosed triangles are hatched.

elucidating the underlying physical mechanisms. A total of six sensitivity experiments were conducted, testing the impacts of latent heat release, surface fluxes of heat and moisture and surface friction.

None of the experiments was able to capture fully the rapidity and intensity of the development, but all three cases that included condensation heating produced major cyclones and featured deepening rates that were more than sufficient to qualify the simulated storms as explosively deepening cyclones. Moreover, the forecasted movements of the storms were in close agreement with the observed movement. The success of the control run - a full physics experiment with explicit or resolvable scale precipitation only - in reproducing detailed features of the storm structure (e.g. boundaries of the main cloud masses) was documented. This success, in conjunction with the satisfactory predictions of movement and intensity, provides grounds for believing that the experimental results yield meaningful information regarding the mechanisms involved in the actual storm development.

The sensitivity experiments revealed the crucial role of latent heat release in promoting rapid deepening. Although the storm development took place in a highly baroclinic environment, the baroclinity was not in itself sufficient to produce a rapidly deepening system in the absence of latent heat addition. A "dry" run with full model physics (other than latent heat

release) yielded a deepening of only 14 mb in 24h. The simulations with latent heating, on the other hand, yielded deepenings of 30-31 mb in the same time interval. The omission of surface fluxes of sensible and latent heat had little impact on either the dry or wet simulations.

The rapid growth of low-level vorticity in the wet simulations implied the existence of strong vortex tube stretching of the boundary layer air and associated strong upward motions in the vicinity of the surface. A cross section taken through the simulated storm midway through the 24h period did indeed reveal the presence of a narrow, sloping, jet-like current of rising air with upward speeds in excess of 0.5 m s^{-1}. This current was located in a region of weak moist static stability and, more significantly, occurred within air that was moist symmetrically neutral or even slightly unstable. By following trajectories it was ascertained that individual parcels in the interior of the low acquired their large vorticities in a very short time interval - only 3-4 hours.

From the foregoing results it appears that the rapid deepening in the control experiment can be attributed to strong low-level ascent and associated large low-level condensation heating within a symmetrically neutral or unstable air mass. In the experiment with parameterized convection the rapid deepening was delayed, presumably because the heating maximum was located higher in the atmosphere. As the convection stabilized the atmosphere, the non-convective, lower-level heating became more prominent and the deepening rate increased accordingly. However, the latter conclusion still needs to be confirmed by additional model diagnosis. A discussion of the important effect of the vertical heating profile on cyclone development can be found in Sardie and Warner (1985).

The reason for the inability of the MM4 to capture fully the depth of the storm is not known. Insufficient grid resolution is one possibility. This and other possibilities will be tested in future experimentation.

5. REFERENCES

Anthes, R.A., E.-Y. Hsie and Y.-H. Kuo, 1987: Description of the Penn State/NCAR Mesoscale Model Version 4 (MM4). NCAR Technical Note, NCAR/TN-282+STR, National Center for Atmospheric Research, Boulder, Colorado, 66 pp.

Bennetts, D.A. and B.J. Hoskins, 1979: Conditional symmetric instability - a possible explanation for frontal rainbands. Quart. J. Roy. Meteor. Soc., 105, 945-962.

Blackadar, A.K., 1979: High resolution models of the planetary boundary layer. Advances in Environmental Science and Engineering, 1, No. 1. Pfafflin and Ziegler, eds., Gordon and Breach Sci.Pub., New York, 50-85.

Eliassen, A., 1962: On the vertical circulation in frontal zones. Geofys.Publ., 24 (4), 147-160.

Emanuel, K., 1983: On assessing local conditional symmetric instability from atmospheric soundings. Mon.Wea.Rev., 111, 2016-2033.

Hsie, E.-Y., R.A. Anthes and D. Keyser, 1984: Numerical simulation of frontogenesis in a moist atmosphere. J.Atmos.Sci., 41, 2581-2594.

Reed, R.J. and M.D. Albright, 1986: A case study of explosive cyclogensis in the eastern Pacific. Mon.Wea.Rev., 114, 2297-2319.

Roebber, P.J., 1984: Statistical analysis and updated climatology of explosive cyclones. Mon.Wea.Rev., 112, 1577-1589.

Sardie, J.M., and T.T. Warner, 1985: A numerical study of the development mechanisms of polar lows. Tellus, 37A, 460-477.

Thorpe, A.J. and K. Emanuel, 1985: Frontogenesis in the presence of small stability to slantwise convection. J.Atmos.Sci., 42, 1809-1824.

Zhang, D.-L. and R.A. Anthes, 1982: A high-resolution model of the planetary boundary layer-sensitivity tests and comparisons with SESAME-79 data. J.Appl.Meteor., 21, 1594-1609.